

Slow rate fluctuations in a network of noisy neurons with coupling delay

I. FRANOVIĆ¹ and V. KLINSHOV²

¹ *Scientific Computing Laboratory, Center for the Study of Complex Systems, Institute of Physics Belgrade, University of Belgrade - Pregrevica 118, 11080 Belgrade, Serbia*

² *Institute of Applied Physics of the Russian Academy of Sciences - 46 Ulyanov Street, 603950 Nizhny Novgorod, Russia*

received 18 September 2016; accepted in final form 6 December 2016
published online 28 December 2016

PACS 87.19.1j – Neuronal network dynamics

PACS 05.40.Ca – Noise

PACS 02.30.Ks – Delay and functional equations

Abstract – We analyze the emergence of slow rate fluctuations and rate oscillations in a model of a random neuronal network, underpinning the individual roles and interplay of external and internal noise, as well as the coupling delay. We use the second-order finite-size mean-field model to gain insight into the relevant parameter domains and the mechanisms behind the phenomena. In the delay-free case, we find an intriguing paradigm for slow stochastic fluctuations between the two stationary states, which is shown to be associated to noise-induced transitions in a double-well potential. While the basic effect of coupling delay consists in inducing oscillations of mean rate, the coaction with external noise is demonstrated to lead to stochastic fluctuations between the different oscillatory regimes.

Copyright © EPLA, 2016

Spontaneous activity of cortical neurons may be characterized as a doubly stochastic process, reflected in a high spike-train variability on a short timescale [1], and *slow* irregular firing rate fluctuations on longer timescales [2,3]. Such slow fluctuations with typical frequencies of $\sim 0.4\text{--}2$ Hz are recorded via EEG or in measurements of local field potentials as the network-level events [4,5], which comprise “on” episodes of high spiking and synaptic activity interspersed with “off” episodes of relative quiescence [6]. The dynamical substrate behind the associated transitions lies in coherent switching of individual neurons between the supra-threshold depolarized “up” states [7,8] and the hyperpolarized “down” states of membrane potential [9]. Alternation of “up” and “down” states [10–12] is a pervasive phenomenon found in sensory, motor, associative and executive cortical areas during sleep [13], under anesthetized [14] and awake conditions [15], as well as in the case of *in vitro* preparations under different experimental protocols [16–18]. Assuming a number of prominent functional roles, slow rate fluctuations are deemed likely to contribute to cortical response variability [19], and have further been found to mediate certain forms of learning and memory [20–24].

In spite of an extensive experimental account, a comprehensive theoretical insight into the described phenomena is still lacking. In this letter, we report on generic mechanisms behind slow rate fluctuations in large neuronal assemblies by focusing on specific roles and interplay of external and intrinsic neuronal noise [25–27], as well as the coupling delay [28,29]. The individual impact of these three ingredients and their co-effects are investigated in this context for the first time.

Note that the terminology concerning the collective dynamics of the network model is fixed as follows. The term “oscillations of mean rate”, or briefly “rate oscillations”, will be reserved for the delay-induced *regular* oscillations of the mean (assembly-averaged) rate. Nonetheless, the slow fluctuations of the network mean rate that emerge in the presence of noise between the two deterministic attractors, be they the two fixed points (analogues of the “up” and the “down” state in our model), or the two limit cycles, will be referred to as the “slow stochastic fluctuations”. In order to analyze the latter, we derive a second-order stochastic mean-field model for the collective network dynamics. It will be demonstrated that the stability and bifurcation analysis of the effective model can

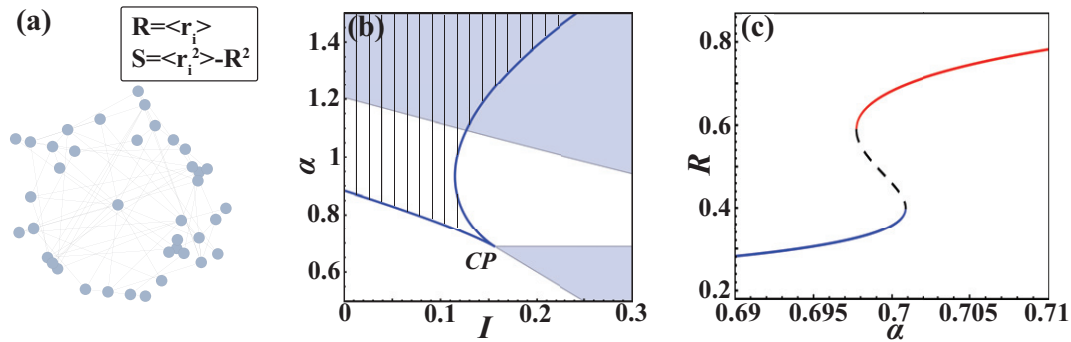


Fig. 1: (Color online) (a) Scheme of a network model. (b) Bifurcation diagram on the I - α plane obtained for the mean-field model at $\tau = 0$ and fixed $B = 0.004$. The “up” and the “down” states coexist in the hatched region between the two branches of saddle-node bifurcations (solid lines). The latter meet at a cusp point (CP), where the pitchfork bifurcation occurs. Within the shaded domain, the condition $\omega^2 > 0$ is satisfied, such that the system may undergo Hopf bifurcation for $\tau > 0$. (c) $R(\alpha)$ bifurcation diagram determined analytically for the mean-field model at $\tau = 0$ and fixed $B = 0.004$, $I = 0.15$. The “up” state (red line) and the “down” state (blue line) are separated by the unstable state (dashed line). The system lies in the close vicinity of the cusp point.

be applied to infer the parameter domains relevant for the slow rate fluctuations.

Our use of the mean-field approach can be interpreted in the context of recent research, where the interest has shifted from classical problems treated by deterministic neural field models [30–33] to a corpus of issues related to how fluctuations and correlations affecting individual neurons are translated to a network level, inducing or modifying the different forms of collective behavior [34,35]. Techniques applied to derive *stochastic* mean-field models can broadly be cast in two classes. The “top-down” framework features perturbation techniques, such as system-size expansion or field-theory methods [34,36], whereas the “bottom-up” strategies, implemented by the population density method [37] or the augmented moment approach [38], involve building a macroscopic model from stochastic equations for local processes. Our derivation pertains to the latter category, containing certain novelties which are indicated below.

Model. – We consider a population of N excitatory neurons following a rate-based dynamics given by [39–41]

$$\frac{dr_i}{dt} = -\lambda r_i + \mathcal{H}(\kappa u_{i,\tau} + I + \sqrt{2B}\eta_i) + \sqrt{2D}\xi_i, \quad (1)$$

where unit indices belong to a $i \in \{1, \dots, N\}$ range, while λ and I stand for the relaxation rate and the bias current, respectively. Note that κ denotes a normalized coupling coefficient $\kappa = c/N$, with c being the coupling strength. The coupling delay, referred to as τ , is assumed to be uniform over the network. Each neuron i receives from the network an input $u_{i,\tau} = \sum_j a_{ij} r_{j,\tau}$, whereby a shorthand notation $r_{j,\tau} \equiv r_j(t - \tau)$ is introduced for the delayed variables. The interaction topology, specified by the elements of the adjacency matrix $a_{ij} \in \{0, 1\}$, conforms to a random network with connectedness probability $p \sim 0.1$ – 0.2 , see fig. 1(a). Although recent experiments provide evidence

for nonrandom structure of neural circuits even on microscopic level [42,43], sparse random architecture maintains a degree of biological plausibility [44] and has been adopted as paradigmatic [37,45,46].

The gain function \mathcal{H} is generally a nonlinear function, which can be explicitly determined for the particular models of spiking neurons [37,46]. The local dynamics is influenced by two independent sources of noise. The external noise η_i , which is attributed intensity B , is associated to fluctuating synaptic input from the embedding environment, whereas the intrinsic noise ξ_i , assigned with intensity D , primarily derives from the stochastic dynamics of ion-channels.

The network dynamics is analyzed via a second-order stochastic mean-field model that incorporates an implicit Gaussian closure hypothesis, in a sense that the mean rate $R(t) = \frac{1}{N} \sum_i r_i(t)$ and the associated variance $S(t) = \frac{1}{N} \sum_i r_i(t)^2 - R(t)^2$ are considered sufficient to describe the system’s macroscopic behavior [47–51]. The detailed derivation of the mean-field model in the case of instantaneous couplings ($\tau = 0$) has been carried out in our previous paper [41]. Given that generalization to the case of delayed couplings proceeds in a fashion analogous to [41], here we only summarize the main points and provide the resulting equations.

The key elements in the derivation of R dynamics include i) the Ansatz that the local variables may be written as $r_i = R + \sqrt{S}\rho_i$, where ρ_i are uncorrelated variables with zero mean and unit variance [52], and ii) the development of the gain function into Taylor series about the average input $X = cpR + I$ for the neurons within the network. In [41], we have argued that the approximation regarding the character of $\{\rho_i\}$ holds under two conditions: first, that the distribution of inward connectivity degrees is sufficiently narrow so that the distribution of r_i is unbiased, and second, that the fraction of shared input between any two neurons is small, which renders their

outputs uncorrelated. Given that the fraction of shared input between any two neurons is p , and that the coefficient of variation for the number of incoming connections amounts to $\sqrt{(1-p)/pN}$, one estimates that the two conditions above will be met if i) the connectivity is small, $p \ll 1$, and ii) the network is sufficiently large, $N \gg 1/p$. In terms of practical application, in [41] we have further numerically verified that the validity of the mean-field approximation for $p = 0.2$ (the value kept fixed throughout this Letter) begins to degrade considerably if the network size is smaller than $N \approx 70$.

Taking the assembly average of eq. (1) and neglecting the terms $\mathcal{O}(1/N^2)$, one ultimately arrives at

$$\frac{dR}{dt} = -\lambda R + H(X_\tau) + \frac{G_\tau}{N} + \sqrt{\frac{\Psi_\tau}{N}} \zeta. \quad (2)$$

In eq. (2), we have used the notation $H(X_\tau) = \mathcal{H}(X_\tau) + B\mathcal{H}''(X_\tau)$, $G_\tau = c^2\mathcal{H}''(X_\tau) [p(1-p)R_\tau^2 + pS_\tau]$, and $\Psi_\tau = 2D + [2B + c^2p^2S_\tau] (\mathcal{H}'(X_\tau))^2$, where $\mathcal{H}'(X_\tau) \equiv \frac{d\mathcal{H}}{dX}(X_\tau)$ and $\mathcal{H}''(X_\tau) \equiv \frac{d^2\mathcal{H}}{dX^2}(X_\tau)$. The variable ζ is a Gaussian white noise that accounts for the joint macroscopic effect of several noisy terms. In particular, the three terms in Ψ_τ describe the impact of the internal noise, the external noise, and the so-called network noise, respectively, whereby the latter derives from fluctuations of the neurons' output signals. Note that the indicated noise terms can be grouped together because their sources are independent by construction of the model.

Derivation of dynamics for the variance requires taking the appropriate Itô derivatives, whereby the final result reads

$$\frac{dS}{dt} = -2\lambda S + 2D + 2B(\mathcal{H}'(X))^2. \quad (3)$$

Note that S affects R dynamics only via an $\mathcal{O}(1/N)$ term, cf. eq. (2). For this reason, we can neglect the impact of the terms $\mathcal{O}(1/N)$ in the evolution of S .

In the thermodynamic limit $N \rightarrow \infty$, the mean-field model comprised of (2) and (3) is completely deterministic, with R dynamics being independent of S . For large but finite N , the finite-size effects become manifest in a twofold fashion. First, a deterministic correction term G_τ/N emerges, which only marginally changes the r.h.s. of eq. (2). The more important finite-size effects in eq. (2) are associated to the stochastic term of intensity Ψ_τ/N . In what follows, it will be demonstrated that the latter can under certain conditions give rise to slow rate fluctuations.

Our approach will consist in carrying out the stability and bifurcation analysis of the mean-field model in the limit $N \rightarrow \infty$ in order i) to gain insight into the parameter domains which admit the slow fluctuations of the mean rate in the case $\tau = 0$, as well as ii) to outline the regions that facilitate the delay-induced oscillations and the stochastic fluctuations between the different oscillatory regimes for $\tau > 0$. Before proceeding, in analogy to [41], we specify the particular form of the gain

function as

$$\mathcal{H}(X) = \begin{cases} 0, & X \leq 0, \\ 3X^2 - 2X^3, & 0 < X < 1, \\ 1, & X \geq 1. \end{cases} \quad (4)$$

Analysis for thermodynamic limit. – As indicated above, in the thermodynamic limit the evolution of R becomes independent of S . Given the gain function (4), it is convenient to introduce a compound connectivity parameter $\alpha = cp$ and rewrite (2) in terms of X , which yields

$$\frac{dX}{dt} = -2\alpha X_\tau^3 + 3\alpha X_\tau^2 - 12\alpha B X_\tau - X + 6\alpha B + I. \quad (5)$$

In the absence of delay, one may show that (5) always admits at least one stable stationary state. For fixed B , X dynamics undergoes a codimension-2 pitchfork bifurcation at $\alpha_p = 2/[3(1-8B)]$ and $I_p = (1-\alpha_p)/2$, where two stable fixed points emerge separated by an unstable one, cf. fig. 1(b) and fig. 1(c). The incipient bistable regime involves the coexistence of the states of higher and lower R , which one may refer to as the “up” and the “down” state, respectively. Figure 1(b) indicates that (I_p, α_p) is actually a cusp point, *viz.* the locus where two saddle-node bifurcation curves meet. Thus, for $\alpha < \alpha_p$, the mean-field model has a unique stable fixed point, whereas for $\alpha > \alpha_p$, it exhibits bistability within a “bistability tongue”. The latter is delineated by the saddle-node bifurcations where the “up” state is born or the “down” state is annihilated. Increasing α in the tongue area reduces R of the unstable state. This has the effect of constricting the attraction basin of the “down” state, such that the “up” state becomes a prevailing feature.

In the presence of coupling delay, eq. (5) is found to undergo Hopf bifurcation for $\tau = \frac{1}{\omega} \arctan(-\omega)$, where $\omega^2 = [6\alpha(X_0^2 - X_0 + 2B)]^2 - 1$, with X_0 denoting the fixed-point solution. The condition $\omega^2 > 0$ can be used to determine the parameter regions admitting such a scenario, cf. the shaded domain in fig. 1(b). Note that enhancing τ may give rise to Hopf bifurcation regardless of whether the delay-free system is monostable or bistable for the given parameter set (α, B, I) . The bifurcation diagram in fig. 2 refers to the case where the delay-free system is monostable, whereas fig. 3(a) concerns the bistable case. In the latter instance, we find that only the “up” state may undergo Hopf bifurcation, which results in a coexistence of the “down” state and the limit cycle.

For both the scenarios above, we have verified that the exact system displays the behavior qualitatively analogous to that of the mean-field model, see fig. 3(b). An important point is that the mean-field model correctly anticipates not only the stationary states, but also the creation of stable limit cycles, which we interpret as the onset of mean rate oscillations. Interestingly, Hopf bifurcation is not the only mechanism giving rise to rate oscillations. In particular, an increase of τ may as well lead to global fold-cycle bifurcations, where a stable and a saddle cycle are born. As a corollary, one finds windows of *bistable rate*

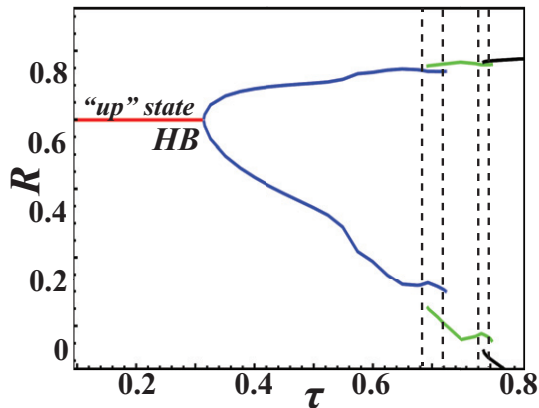


Fig. 2: (Color online) Bifurcation diagram $R(\tau)$ numerically obtained for the mean-field model under the parameter set $I = 0.03$, $B = 0.001$, $\alpha = 2.165$, $N = 400$. The horizontal line corresponds to the “up” state, which is destabilized via Hopf bifurcation (HB). The oscillatory solutions above HB are represented by the corresponding amplitudes. Within the two τ intervals indicated by the dashed lines, the mean-field model exhibits bistability between the two limit cycles, which is associated to the occurrence of fold-cycle bifurcations.

oscillations with different amplitudes, cf. the two intervals indicated by the dashed lines in fig. 2. Note that in the interval around $\tau \approx 0.7$, the saddle cycle acts as a separatrix between the cycle created via Hopf bifurcation and the stable cycle emerging from the fold-cycle bifurcation, whereby the latter has a larger amplitude. The bistability windows terminate in a scenario involving the inverse fold-cycle bifurcation, where the stable cycle with a smaller amplitude vanishes by colliding with the saddle cycle. Below we show that the mean-field model provides meaningful insights even for such complex dynamical regimes.

Slow rate fluctuations. – Having analyzed the mean-field model in the limit $N \rightarrow \infty$, one is able to anticipate the parameter regions where the exact system is likely to exhibit slow stochastic fluctuations of mean rate. Such a nontrivial behavior can be expected in the domains promoting bistable dynamics for the thermodynamic limit.

Let us first consider the case $\tau = 0$. Here, the mechanism behind slow rate fluctuations may be explained by invoking the paradigm of a noise-driven particle fluctuating between the minima of a double-well potential. In the domains where the mean-field model possesses two stable stationary states for $N \rightarrow \infty$, each of them may be associated to a minimum of the potential, while the separatrix provides for the barrier. The noisy term emerging for finite N can then facilitate transitions between the wells.

In order to obtain the form of the potential guiding the system dynamics, we use the adiabatic approximation, which consists in replacing S by its stationary value $S_0 = D + B(\mathcal{H}'(X))^2$ given by (3). Substituting this in (2) and rewriting the latter in terms of X , one obtains

$$\frac{dX}{dt} = -\frac{dV}{dX} + \sqrt{\Phi}\zeta. \quad (6)$$

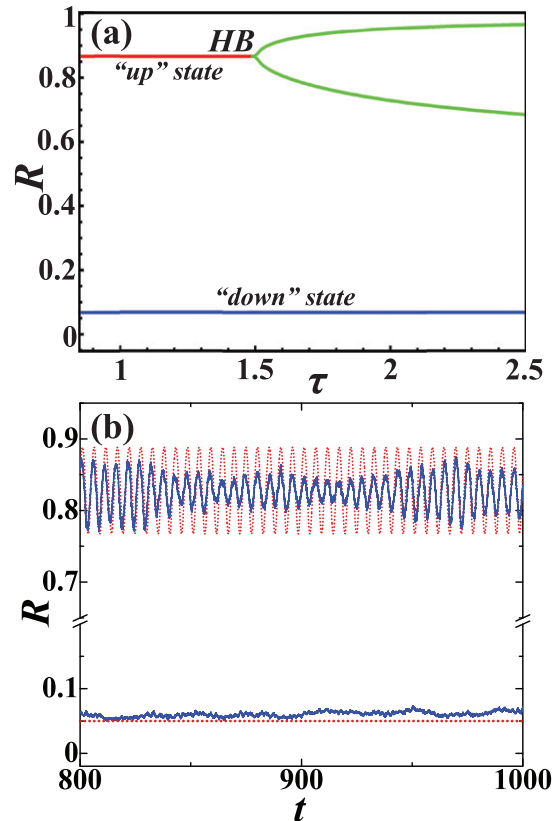


Fig. 3: (Color online) (a) Bifurcation diagram $R(\tau)$ numerically obtained for the mean-field model under the parameter set $I = 0.06$, $\alpha = 1.3$, $B = 0.002$. The horizontal lines denote the levels of the “down” (blue line) and the “up” state (red line), whereby the latter undergoes Hopf bifurcation (HB) at $\tau = 1.495$. The oscillatory solutions above HB are represented by the associated amplitudes (green lines). (b) $R(t)$ series of the exact system (blue solid lines) and the mean-field model (red dotted lines) illustrate a bistable regime involving the coexistence of the oscillatory solution and the “down” state. The results are obtained for $\tau = 1.9$ and $N = 400$, with the remaining parameters being the same as in (a).

Here, $V(X) = \alpha X^4/2 - \alpha X^3 + (6\alpha B + 1)X^2 - (6\alpha B + I)X + \mathcal{O}(1/N)$, whereas the macroscopic noise is given by $\Phi = \alpha^2(2 + \alpha^2) [36BX^2(1 - X)^2 + D]/N$. The potential $V(X)$ has a double-well form above the pitchfork bifurcation. Note that the switching between the minima of $V(X)$ should unfold in a sufficiently close vicinity of the pitchfork bifurcation, because too far above it, the barrier becomes too high for the noisy term to overcome it.

As expected, we have found slow rate fluctuations by numerical simulations of the exact system within the indicated parameter region. There, the typical $X(t)$ series, such as the one in fig. 4(a), can be described as alternations between the “up” and the “down” state of the mean-field model. This is corroborated by the bimodal form of the probability distribution $f(X)$ obtained from the $X(t)$ series, cf. fig. 4(b). The corresponding $V(X)$ is plotted in the same figure in order to illustrate that the coordinates

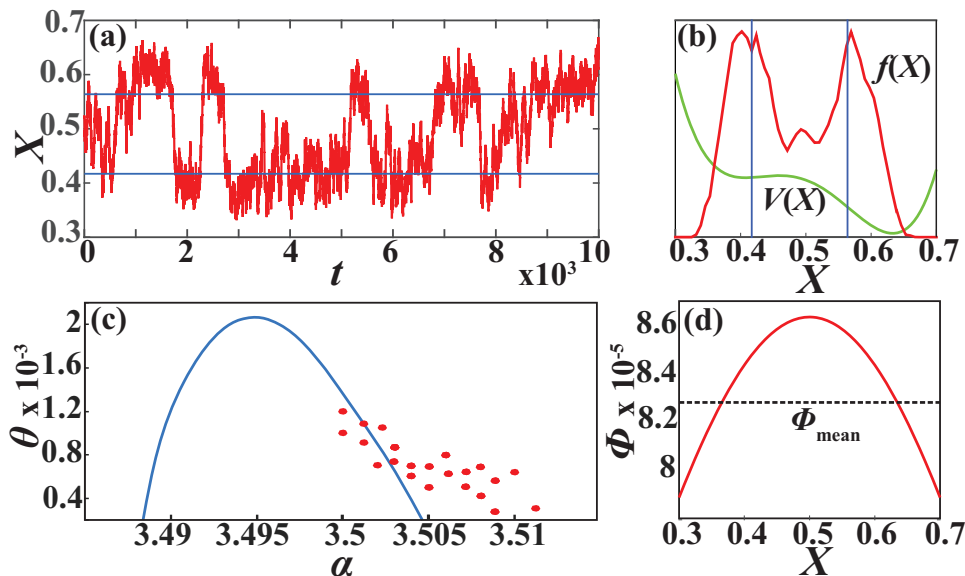


Fig. 4: (Color online) (a) Slow rate fluctuations in the $X(t)$ series of a network of $N = 400$ neurons with parameters $B = 0.004$, $D = 0.02$, $\alpha = 0.7$, $I = 0.1505$. The latter are the same as in fig. 1(c). Horizontal lines indicate the levels associated to “up” and “down” states of the mean-field model. (b) $V(X)$ denotes the potential for the mean-field model, whereas $f(X)$ presents the histogram obtained from the $X(t)$ series from (a). (c) The solid line and the dots refer, respectively, to the dependences $\theta(\alpha)$ obtained analytically for the mean-field model and numerically for the exact system. (d) $\Phi(X)$ determined analytically for the mean-field model (6). The network parameters in (b)–(d) are adopted from (a).

of $f(X)$ maxima approximately coincide with the location of wells of $V(X)$.

The slow rate fluctuations are observed in a confined parameter region, as shown in fig. 4(c). The dots indicate the numerically determined transition rate θ for the exact system as a function of the coupling parameter α . Using the mean-field model, one is further able to estimate θ analytically. In this context, first note that the noise intensity in eq. (6) depends on X , which implies that $V(X)$ has a fluctuating barrier. Nevertheless, in a first approximation, the problem may be reduced to the scenario with a stationary barrier. To justify this, we have plotted in fig. 4(d) the dependence $\Phi(X)$ for the parameter set from fig. 4(a). One learns that Φ is bounded for X values between the wells, such that the average value Φ_{mean} can be taken as representative. Since the noise intensity is sufficiently small compared to the barrier height, the mean first-passage time from one well to the other may be estimated by the Kramers formula [53,54],

$$T_{X_{\pm} \rightarrow X_{\mp}} \approx \frac{\pi}{\sqrt{|V''(X_u)|V''(X_{\pm})}} \exp \left[\frac{V(X_u) - V(X_{\pm})}{\Phi_{mean}} \right]. \quad (7)$$

Here, X_- (“down” state) and X_+ (“up” state) refer to coordinates of minima of $V(X)$, whereas X_u is the location of its maximum. The total transition rate θ is then given by $\theta = 1/(T_{X_+ \rightarrow X_-} + T_{X_- \rightarrow X_+})$. The solid line in fig. 4(c) shows the dependence $\theta(\alpha)$ obtained for the mean-field model by applying the described approximation. Note that the indicated α interval where θ is positive lies quite close to the one where the exact system exhibits

rate fluctuations. Moreover, the θ values estimated analytically are of the same order as those observed numerically, which further evinces that the mean-field model predicts the behavior of the exact system in a satisfactory fashion. The point that their matching is only qualitative reflects the fact that the mean-field model becomes less accurate in the vicinity of the pitchfork bifurcation [41].

The mean-field model can also account for the mechanism behind more intricate slow rate fluctuations observed in the presence of coupling delays ($\tau > 0$). In particular, it allows one to predict the occurrence of stochastic switching between the different oscillatory solutions. These transitions take place in the parameter domain where the mean-field model possesses two coexisting stable oscillatory solutions for $N \rightarrow \infty$, cf. fig. 2. An example of such solutions is illustrated in fig. 5(a) for $\tau = 0.7$ and the remaining parameters fixed as in fig. 2. Note that the oscillations of larger (smaller) amplitude correspond to a limit cycle born via a global fold-cycle (Hopf) bifurcation. For the given parameter set, we find that the exact system displays large fluctuations of mean rate, cf. fig. 5(b). These fluctuations may be interpreted as noise-induced switching between the two oscillatory solutions.

Nevertheless, one also observes that the matching between the dynamics of the mean-field model and the exact system is qualitative, but rather lacks the quantitative character. In particular, the amplitudes of the two solutions found for the mean-field model are quite close, whereas the characteristic amplitudes of the two oscillatory regimes involved in slow stochastic fluctuations for

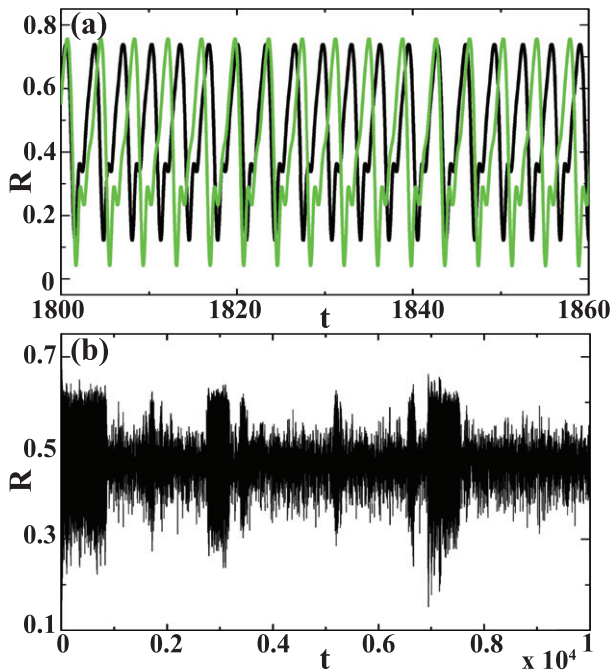


Fig. 5: (Color online) (a) Bistable dynamics of the mean-field model characterized by the coexistence of two limit cycles. The cycle with larger amplitude (green line) is born via the fold-cycle bifurcation, whereas the solution of smaller amplitude (black line) derives from the Hopf bifurcation. The delay is set to $\tau = 0.7$, while the rest of parameters are as in fig. 2. (b) $R(t)$ series for the network of $N = 400$ neurons shows slow stochastic fluctuations for the parameter set from (a).

the exact system are much further apart, cf. fig. 5(a) and fig. 5(b). This discrepancy derives from the general fact that the system becomes quite sensitive to small perturbations in the vicinity of a bifurcation, which severely affects the validity of the effective model. In this case, the role of such small perturbations is assumed by the finite-size effects. Note that we have already shown in [41] that the finite-size effect grows so large in the vicinity of a pitchfork bifurcation that one cannot use simple linearization to estimate it. We suspect that essentially the same scenario occurs here as the system in fig. 5 lies close to a fold-cycle bifurcation.

Discussion. – We have demonstrated how the individual and combined effects of different noise terms and coupling delay give rise to slow fluctuations of mean rate in a random neural network. It has been shown that the generic mechanisms and the underlying statistical features can be qualitatively accounted for by looking into the appropriate second-order stochastic mean-field model. In the delay-free case, the basic scenario behind slow rate fluctuations may be characterized as noise-driven transitions of a particle in a double-well potential. In the thermodynamic limit, the mean-field model displays bistability between the “up” and the “down” state, whereas the finite-size effect consists in introducing a noise term that induces transitions between the metastable states. Apart from

anticipating the parameter domains that promote rate fluctuations, the analysis of the mean-field model has allowed us to estimate the associated transition rates.

Our results further indicate that introducing coupling delays into the network model facilitates the emergence of mean rate oscillations. An interesting finding is that the cooperative action of noise and delay may lead to slow fluctuations that can be interpreted as stochastic mixing between two different oscillatory regimes. The predictions of the mean-field model remain qualitatively valid even for such unexpected scenarios.

It is relevant to estimate how the typical durations of “up” and “down” states from our simulations compare to lifetimes of such states in biological networks, which are established to comprise a range from several hundred ms up to ~ 2 s [12]. In order to do so, we take into account that the time constant $\tau_m = 1/\lambda$ should be of the order of 1 ms [55,56], from where one may infer that a time unit in eq. (1) roughly corresponds to $\sim 10^{-3}$ s. Thus, when translated to real time units, the residence times observed in fig. 4(c) span the range of about 800–2000 ms, which approximately coincide with a biologically plausible range.

So far, two alternative scenarios have been suggested in modeling studies to explain for the occurrence of rate fluctuations, emphasizing either the impact of synaptic plasticity or the network topology. By the first scenario, cycling of “up” and “down” states is promoted by a mechanism based on short-term synaptic depression [57,58], whereby the extinction of “up” state is triggered by the activity-dependent self-inhibition. By the other scenario, slow rate fluctuations emerge in balanced excitatory-inhibitory networks [45,59,60], if the latter embed clustered subnetworks [2]. In principle, an analogous form of behavior can also be recovered for balanced networks in the vicinity of transition to chaos [61]. At variance with our approach, prior studies have not explicitly addressed the influence of noise, either in the onset of the rate fluctuations or the underlying statistics. Also, the previous research does not refer to the effects of coupling delay.

An important open question is whether and how more complex network topologies would affect the robustness of rate fluctuations. In our setup with random topology, the effect is relatively sensitive to parameter values. However, given the recent report that the macroscopic rate fluctuations are robust in balanced networks with embedded clusters [2], we have begun to develop a mean-field model for networks with an excitation-inhibition balance and clustered architecture. We believe that the mean-field approach will allow us to gain a deeper understanding of the relation between the network structure and the slow rate fluctuations.

This work is supported by the Ministry of Education, Science and Technological Development of Republic of Serbia under project No. 171017, by the Russian Foundation for Basic Research within Grants Nos. 14-02-00042

and 15-02-04245, and by the Ministry of Education and Science of the Russian Federation, Agreement No. MK-8460.2016.2.

REFERENCES

- [1] DESTEXHE A., RUDOLPH M. and PARÉ D., *Nat. Rev. Neurosci.*, **4** (2003) 739.
- [2] LITWIN-KUMAR A. and DOIRON B., *Nat. Neurosci.*, **15** (2012) 1498.
- [3] CHURCHLAND M. M. *et al.*, *Nat. Neurosci.*, **13** (2010) 369.
- [4] BUZSÁKI G., *Rhythms of the Brain* (Oxford University Press, Oxford) 2006.
- [5] BUZSÁKI G., ANASTASSIOU C. A. and KOCH C., *Nat. Rev. Neurosci.*, **13** (2012) 407.
- [6] VYAZOVSKIY V. V. and HARRIS K. D., *Nat. Rev. Neurosci.*, **14** (2013) 443.
- [7] HAHN T. T. G., SAKMANN B. and MEHTA M. R., *Nat. Neurosci.*, **9** (2006) 1359.
- [8] GIGANTE G., DECO G., MAROM S. and DEL GIUDICE P., *PLoS Comput. Biol.*, **11** (2015) e1004547.
- [9] COWAN R. L. and WILSON C. J., *J. Neurophysiol.*, **71** (1994) 17.
- [10] MILLMAN D., MIHALAS S., KIRKWOOD A. and NIEBUR E., *Nat. Phys.*, **6** (2010) 801.
- [11] MCCORMICK D. A., MCGINLEY M. J. and SALKOFF D. B., *Curr. Opin. Neurobiol.*, **31** (2015) 133.
- [12] HAHN T. T. G. *et al.*, *Nat. Neurosci.*, **15** (2012) 1531.
- [13] STERIADE M., MCCORMICK D. A. and SEJNOWSKI T. J., *Science*, **262** (1993) 679.
- [14] ANDERSON J. *et al.*, *Nat. Neurosci.*, **3** (2000) 617.
- [15] PETERSEN C. C. H. *et al.*, *Proc. Nat. Acad. Sci. U.S.A.*, **100** (2003) 13638.
- [16] COSSART R., ARONOV D. and YUSTE R., *Nature*, **423** (2003) 283.
- [17] SANCHEZ-VIVES M. V. and MCCORMICK D. A., *Nat. Neurosci.*, **3** (2000) 1027.
- [18] SHU Y., HASENSTAUB A. and MCCORMICK D. A., *Nature*, **423** (2003) 288.
- [19] GHORBANI M., MEHTA M., BRUINSMA R. and LEVINE A. J., *Phys. Rev. E*, **85** (2012) 021908.
- [20] JI D. and WILSON M. A., *Nat. Neurosci.*, **10** (2007) 100.
- [21] MARSHALL L., HELGADÓTTIR H., MÖLLE M. and BORN J., *Nature*, **444** (2006) 610.
- [22] DIEKELMANN S. and BORN J., *Nat. Rev. Neurosci.*, **11** (2010) 114.
- [23] HEIB D. P. J. *et al.*, *PLoS ONE*, **8** (2013) e82049.
- [24] MIYAMOTO D. *et al.*, *Science*, **352** (2016) 1315.
- [25] McDONNELL M. D. and WARD L. M., *Nat. Rev. Neurosci.*, **12** (2011) 415.
- [26] FAISAL A. A., SELEN L. P. J. and WOLPERT D. M., *Nat. Rev. Neurosci.*, **9** (2008) 292.
- [27] ANISHCHENKO V. S., ASTAKHOV V., NEIMAN A., VADIVASOVA T. and SCHIMANSKY-GEIER L., *Nonlinear Dynamics of Chaotic and Stochastic Systems* (Springer, Berlin, Heidelberg) 2007.
- [28] PIKOVSKY A., ZAIKIN A. and DE LA CASA M. A., *Phys. Rev. Lett.*, **88** (2002) 050601.
- [29] SCHÖLL E., HILLER G., HÖVEL P. and DAHLEM M. A., *Philos. Trans. R. Soc. A*, **367** (2009) 1079.
- [30] FOLIAS S. E. and BRESSLOFF P. C., *Phys. Rev. Lett.*, **95** (2005) 208107.
- [31] PINTO D. J. and ERMENTROUT G. B., *SIAM J. Appl. Math.*, **62** (2001) 206.
- [32] LAING C. R., TROY W. C., GUTKIN B. and ERMENTROUT G. B., *SIAM J. Appl. Math.*, **63** (2002) 62.
- [33] JIRSA V. K. and HAKEN H., *Physica D*, **99** (1997) 503.
- [34] BRESSLOFF P. C., *SIAM J. Appl. Math.*, **70** (2009) 1488.
- [35] BRESSLOFF P. C., *Phys. Rev. E*, **82** (2010) 051903.
- [36] BUICE M. A. and COWAN J. D., *Phys. Rev. E*, **75** (2007) 051919.
- [37] BRUNEL N. and HAKIM V., *Neural Comput.*, **11** (1999) 1621.
- [38] HASEGAWA H., *Phys. Rev. E*, **67** (2003) 041903.
- [39] HASEGAWA H., *Phys. Rev. E*, **75** (2007) 051904.
- [40] ANDERSON R. A., MUSALLAM S. and PESARAN B., *Curr. Opin. Neurobiol.*, **14** (2004) 720.
- [41] KLINSHOV V. and FRANOVIĆ I., *Phys. Rev. E*, **92** (2015) 062813.
- [42] SONG S. *et al.*, *PLoS Biol.*, **3** (2005) e68.
- [43] KLINSHOV V., TERAMAE J.-N., NEKORKIN V. and FUKAI T., *PLoS ONE*, **9** (2014) e94292.
- [44] LUCK J. M. and MEHTA A., *Phys. Rev. E*, **90** (2014) 032709.
- [45] VAN VREESWIJK C. and SOMPOLINSKY H., *Neural Comput.*, **10** (1998) 1321.
- [46] LY C. and TRANCHINA D., *Neural Comput.*, **19** (2007) 2032.
- [47] FRANOVIĆ I., TODOROVIĆ K., VASOVIĆ N. and BURIĆ N., *Phys. Rev. E*, **89** (2014) 022926.
- [48] FRANOVIĆ I., TODOROVIĆ K., VASOVIĆ N. and BURIĆ N., *Phys. Rev. E*, **87** (2013) 012922.
- [49] FRANOVIĆ I., TODOROVIĆ K., VASOVIĆ N. and BURIĆ N., *Phys. Rev. Lett.*, **108** (2012) 094101.
- [50] LINDNER B., GARCIA-OJALVO J., NEIMAN A. and SCHIMANSKY-GEIER L., *Phys. Rep.*, **392** (2004) 321.
- [51] ZAKS M. A., SAILER X., SCHIMANSKY-GEIER L. and NEIMAN A. B., *Chaos*, **15** (2005) 026117.
- [52] BURKITT A. N., *Biol. Cybern.*, **95** (2006) 1.
- [53] GARDINER C. W., *Handbook of Stochastic Methods for Physics, Chemistry and the Natural Sciences* (Springer-Verlag, Berlin) 2004.
- [54] PAVLIOTIS G. A., *Stochastic Processes and Applications* (Springer, New York) 2014.
- [55] GERSTNER W. and KISTLER W. M., *Spiking Neuron Models: Single Neurons, Populations, Plasticity* (Cambridge University Press, New York) 2004.
- [56] GERSTNER W., KISTLER W. M., NAUD R. and PANINSKI L., *Neuronal Dynamics: From Single Neurons to Networks and Models of Cognition* (Cambridge University Press, Cambridge) 2014.
- [57] HOLCMAN D. and TSODYKS M., *PLoS Comput. Biol.*, **2** (2006) 174.
- [58] MEJIAS J. F., KAPPEN H. J. and TORRES J. J., *PLoS ONE*, **5** (2010) e13651.
- [59] VOGELS T. P. and ABBOTT L. F., *J. Neurosci.*, **25** (2005) 10786.
- [60] ROSENBAUM R. and DOIRON B., *Phys. Rev. X*, **4** (2014) 021039.
- [61] KADMON J. and SOMPOLINSKY H., *Phys. Rev. X*, **5** (2015) 041030.